Control Over the Branched Structures of Platinum Nanocrystals for Electrocatalytic Applications

Liang Ma,[†,▽] Chengming Wang,[†,▽] Ming Gong,[§] Lingwen Liao,[†] Ran Long,[†] Jinguo Wang,[⊥] Di Wu,[†] Wei Zhong,[†] Moon J. Kim,[⊥,¶,*] Yanxia Chen,[†] Yi Xie,[†] and Yujie Xiong[†,‡,*]

[†]Hefei National Laboratory for Physical Sciences at the Microscale and [§]Laboratory of Engineering and Material Science, University of Science and Technology of China, Hefei, Anhui 230026, P. R. China, [‡]School of Engineering and Applied Science, Washington University in St. Louis, St. Louis, Missouri 63130, United States, [⊥]Department of Materials Science and Engineering, University of Texas at Dallas, Richardson, Texas 75083, United States, and [¶]Department of Nanobio Materials and Electronics, World Class University, Gwangju Institute of Science and Technology, Gwangju 500-712, Korea. [▽]These authors contributed equally to this work.

ABSTRACT Structural control of branched nanocrystals allows tuning two parameters that are critical to their catalytic activity—the surface-to-volume ratio, and the number of atomic steps, ledges, and kinks on surface. In this work, we have developed a simple synthetic system that allows tailoring the numbers of branches in Pt nanocrystals by tuning the concentration of additional HCl. In the synthesis, HCl plays triple functions in tuning branched structures *via* oxidative etching: (i) the crystallinity of seeds and nanocrystals; (ii) the number of {111} or {100} faces provided for growth sites; (iii) the supply kinetics of freshly formed Pt atoms in solution. As a result, tunable Pt branched structures—tripods, tetrapods, hexapods, and octopods with identical chemical environment—can be rationally synthesized in a single system by simply altering the etching strength. The controllability in branched structures enables to reveal that their electrocatalytic performance can be optimized by constructing complex structures. Among various branched structures, Pt octopods exhibit particularly high activity in formic acid oxidation as compared with their counterparts and commercial Pt/C catalysts. It is anticipated that this work will open a door to design more complex nanostructures and to achieve specific functions for various applications.

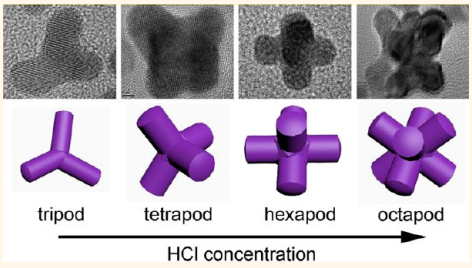

KEYWORDS: platinum · branched structure · HCl · electrocatalysis · nanocrystal

Platinum (Pt) has been widely utilized as a catalyst in reduction of pollutant gases emitted from automobiles, synthesis of nitric acid, oil cracking, ethylene hydrogenation and proton-exchange membrane (PEM) fuel cells.[1−4] It has been proven that the catalytic activities of Pt and other noble metals are highly dependent on their surface structures in formic acid oxidation,[5−9] ammonia oxidation,[10−12] oxygen reduction,[13−15] nitrite reduction,[16−18] and many other reactions.[19−21] In the reaction of formic acid oxidation, Herrero, Iwasita, Hoshi and Markovic *et al.* have demonstrated the importance of controlling surface structures (including facet effect) in tuning catalytic activities with intensive studies on Pt single crystals.[5−9] In recent years, considerable efforts have been made on the use of Pt nanocrystals in various catalytic reactions, mainly due to their high surface-to-volume ratios that are supposed to enable higher activities in catalysis. In particular, Pt nanocrystals enclosed by high-index facets have been of great interests in terms of improving catalytic activities, as this class of facets generally contains a high density of stepped surface atoms.[5] Given that the surface structures of nanocrystals have a strong correlation with their morphologies, morphology control of Pt nanocrystals has become a central theme of research with an ultimate goal to tune the nanocrystal catalytic performance.[22−24] Among various possible morphologies, branched nanostructures (*e.g.*, multipods) are of particular interest owing to their unique surface structures. The parameter control of branched structures allows tuning the surface-to-volume ratios and the number of atomic steps, ledges, and kinks on surface, which can greatly impact the catalytic activity.[25,26]

The morphology of multipods has been commonly observed in the synthesis of II−VI

* Address correspondence to yjxiong@ustc.edu.cn, moonkim@utdallas.edu.

Received for review July 24, 2012 and accepted October 15, 2012.

Published online October 15, 2012
10.1021/nn304237u

semiconductor nanocrystals by controlling the formation of different crystal structures in the same nanocrystal.[27−29] However, as a face-centered cubic (fcc) metal, Pt has no intrinsic driving force for the growth of anisotropic structures when the seeds are surrounded by an isotropic medium in solution phase, making the synthesis of Pt branched structures extremely unfavorable.[22−24] In previous studies, a seeding process was employed as a major method for producing Pt branched structures.[25,26,30,31] In this synthetic system, anisotropic overgrowth of nanocrystals could occur owing to a faster rate of atomic addition than that of atomic diffusion when the concentration of atoms added to seed surface is well controlled. Note that metal salts such as silver and cobalt precursors have been also used as "trace elements" to induce the growth of multipods, which should share similar fundamentals with the seeding process.[32,33] Some other trace metals such as iron species can affect the branched growth *via* a different mechanism by altering reaction kinetics, given their function in oxidative etching.[34] Overall, several different patterns of branched growth in Pt nanocrystals have been observed in various synthetic systems in literature. The growth patterns mainly depend on the crystallinity of seeds (*i.e.*, twinned *versus* single-crystal) and the surface facets activated for atomic addition, which can lead to different numbers of branches in final morphologies.[25,26] For the purpose of designing nanostructures with tunable catalytic performance, it is important to tailor these parameters while maintaining the others constant. For instance, when various branched structures were obtained in different synthetic systems, it could result in varied chemical environments to the nanocrystal surface (*i.e.*, molecules left on surface), which may in turn have significant impact on the catalytic activities of nanocrystals. Thus it is needed to develop a simple but comprehensive system that allows us to tune the parameters of branched structures with a versatile tool indeed. With this system developed, we should be able to investigate how their electrocatalytic performance can be optimized by constructing complex structures, free of the influence from other factors such as the variation in chemical environments on nanocrystal surface.

Herein, we report a facile, one-step synthetic approach to Pt branched nanocrystals with controllable numbers of branches. As compared to the previously reported systems, the present method offers the capability of directly controlling the anisotropic growth of branches on Pt nanocrystals in a single reaction, without the needs of adding seeds or foreign cations. More importantly, multiple different growth patterns of branched structures can be observed by simply tuning the concentration of additional HCl in this system. Thus the synthetic system proposed here not only presents a simpler platform for investigating the formation mechanism of Pt multipods, but provides samples with varied structures and identical chemical environment for catalytic studies. As an example, we demonstrate that the electrocatalytic performance of Pt nanocrystals can be optimized by controlling their branched structures.

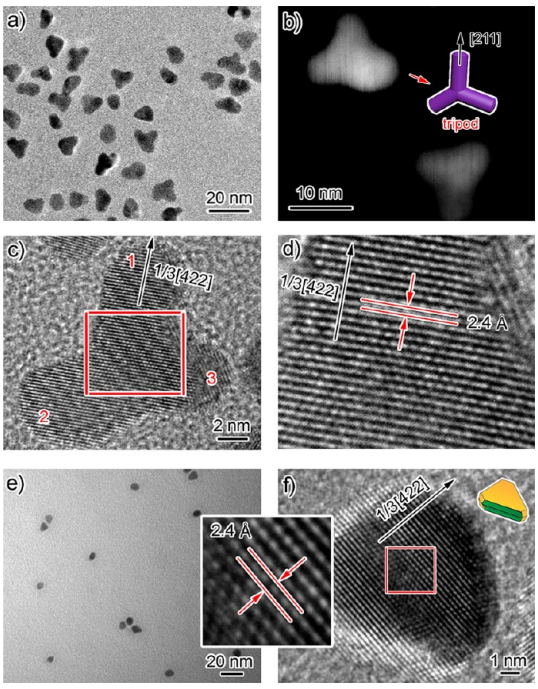

Figure 1. TEM, STEM, and HRTEM images of the tripod sample prepared in the absence of HCl for 24 h: (a) TEM image; (b) STEM image; (c) HRTEM image. The inset of panel b shows the schematics of a typical nanoparticle in the image. The numeric labels in the HRTEM image illustrate the numbers of branches. (d) Magnified image of the region marked by the red box in panel c. (e) TEM image of the intermediate product formed at 30 min. (f) HRTEM image of intermediate product, and the insets show a magnified image and the corresponding structure schematics. The green and orange colors in the schematics represent {100} and {111} facets, respectively. Owing to the difficulty of drawing the exact structures of branched nanocrystals, the schematics in Figures 1−4 only represent the orientation of nanocrystals and do not reflect the true dimensions.

RESULTS AND DISCUSSION

In the present work, Pt branched nanocrystals were grown from a simple reaction system where H_2PtCl_6, poly(vinyl pyrrolidone) (PVP) and KBr were dissolved in a mixed solvent of ethylene glycol and water. PVP was used as a stabilizer to prevent the agglomeration of nanoparticles, while ethylene glycol served as a reducing agent. Different amounts of HCl were added to the reaction system, tuning the crystallinity of seeds and the modes of atomic addition.

We first examined the case in the absence of HCl. Figure 1a shows the transmission electron microscopy (TEM) image of a typical sample obtained at t = 24 h, revealing that the majority of product has three branches with the pod width of about 4 nm. The distance between

the tips of two pods is about 12 nm. This tripod morphology is further confirmed by scanning transmission electron microscopy (STEM, Figure 1b). Furthermore, high-resolution TEM (HRTEM) images in Figure 1c,d have verified the planar structure of this tripod. The observed lattice fringes can be assigned to the forbidden 1/3{422} reflection that has been also observed in metallic nanostructures in the form of thin plates bounded by atomically flat surfaces, indicating the existence of a layer of twin plane in between.[35−38] The growth axis of each pod can be determined to [211], which is consistent with the literature.[26] To elucidate the growth mode of tripods, we have collected samples from different growth stages in the syntheses. Figure 1 panels e and f are typical TEM and HRTEM images of the sample obtained at 30 min. The TEM image reveals that the intermediates consist of truncated triangular or circular nanoplates. The nanoplates are single-twinned with {111} facets as top and bottom surface, as indicated by the HRTEM image. According to the symmetry of fcc structure, their side faces should be a mix of alternated {111} and {100} facets. Comparing the structure of tripods with that of intermediate nanoplates, we can conclude that each pod of a tripod grows along [211] axis from one side {111} face of an intermediate nanoplate. This branched growth is named as "Growth Pattern 1" in our work.

When 112.5 mM HCl was introduced to the reaction, the structure of nanocrystals was tuned from single twin to single crystal as determined by HRTEM images (Figure 2c,d). TEM and STEM images in Figures 2a,b reveal that most nanoparticles in the sample obtained at t = 24 h have four branches with branch distance of *ca.* 15 nm. The growth axis of each branch has been determined to [111] by HRTEM images. Early stage studies indicate that these tetrapods actually evolve from single-crystal cuboctahedral seeds that are enclosed by a mix of {100} and {111} facets (see Figure 2e,f). Since the growth axis of each pod is [111], it is assumed that branch growth occurs on four {111} faces of each cuboctahedral seed. Given that each cuboctahedron possesses eight {111} corners, only half of the corners should have provided sites for atomic addition in the formation of this tetrapod structure. This structure assignment is also well supported by the literature.[32] We mark this growth mode as "Growth Pattern 2" in our work.

As the concentration of HCl was doubled, the resulted nanocrystals maintained the single-crystal structure, but the number of pods was increased to six (see Figure 3a,b for the sample obtained at t = 24 h). The distance between the tips of two pods is roughly 18 nm. HRTEM images in Figure 3c,d reveal that each branch of a hexapod grows along the [100] axis. The precursors for hexapods have been also successfully captured at 15 min, which show the morphology of

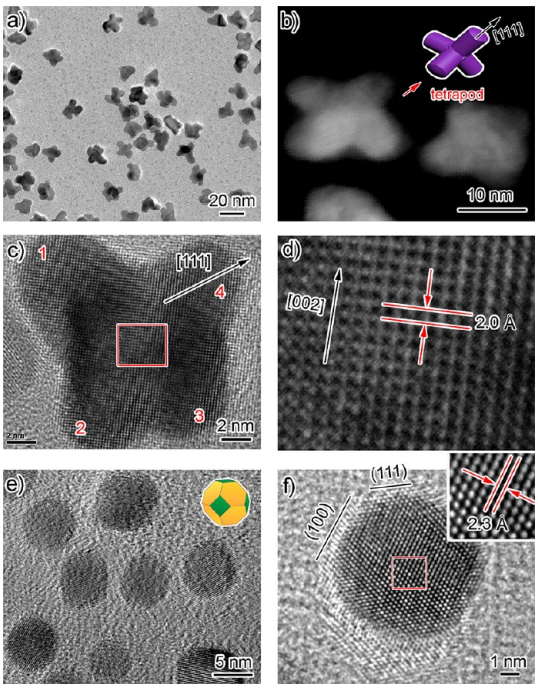

Figure 2. TEM, STEM, and HRTEM images of the tetrapod sample prepared in the presence of 112.5 mM HCl for 24 h: (a) TEM image; (b) STEM image; (c) HRTEM image. The inset of panel b shows the schematics of a typical nanoparticle in the image. The numeric labels in the HRTEM image illustrate the numbers of branches. (d) Magnified image of the region marked by the red box in panel c. (e) TEM image and structure schematics of the intermediate product formed at 15 min. (f) HRTEM image of intermediate product, and the inset is a magnified image of the region in the red box. The green and orange colors in the schematics represent {100} and {111} facets, respectively.

nanospheres (see Figure 3e). HRTEM image in Figure 3f confirms that these nearly spherical nanoparticles have very similar structure to the seeds for tetrapods—cuboctahedrons covered by {100} and {111} facets. Thus we can reach the conclusion that the hexapods are formed *via* atomic addition on the six {100} faces of cuboctahedral seeds. This is the "Growth Pattern 3" observed in our work.

As the amount of HCl was further tripled, the structure of products appeared to be very complex, and the size of nanocrystals was increased to 22 nm (see TEM image in Figure 4a for the sample obtained at t = 24 h). STEM image (Figure 4b) indicates that the nanocrystals may be octopods, because of the appearance of branches and the orientation of nanocrystals. The structure of octopods is further confirmed by HRTEM images (Figure 4c,d) when tilting the sample by 15°. HRTEM also reveals that the nanocrystals are single-crystal and the growth axis of each pod is [111] (see Figure 4e). Since the growth direction is the same as that of a tetrapod, we highly suspect that the growth of each octopod occurs on all the eight {111} corners of a cuboctahedron. To verify this feature, we have attempted to collect intermediates from early stages of reaction. Unfortunately, we have not been able to

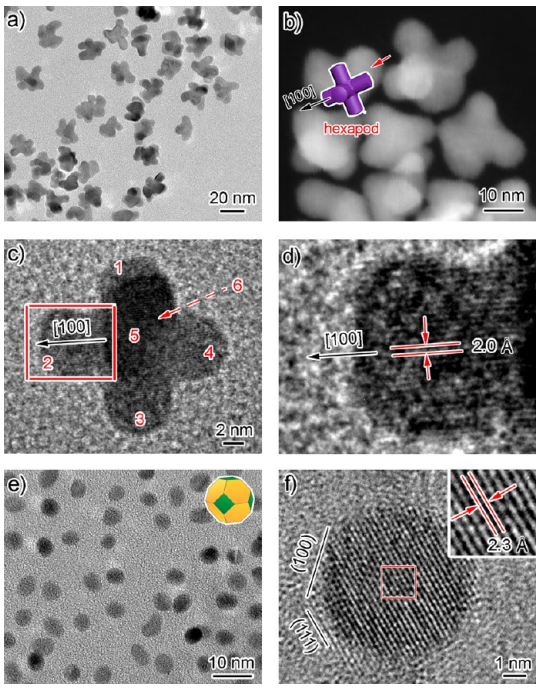

Figure 3. TEM, STEM, and HRTEM images of the hexapod sample prepared in the presence of 225 mM HCl for 24 h: (a) TEM image; (b) STEM image; (c) HRTEM image. The inset of panel b shows the schematics of a typical nanoparticle in the image. The numeric labels in the HRTEM image illustrate the numbers of branches. (d) Magnified image of the region marked by the red box in panel c. (e) TEM image and structure schematics of the intermediate product formed at 15 min. (f) HRTEM image of intermediate product, and the inset is a magnified image of the region in the red box. The green and orange colors in the schematics represent {100} and {111} facets, respectively.

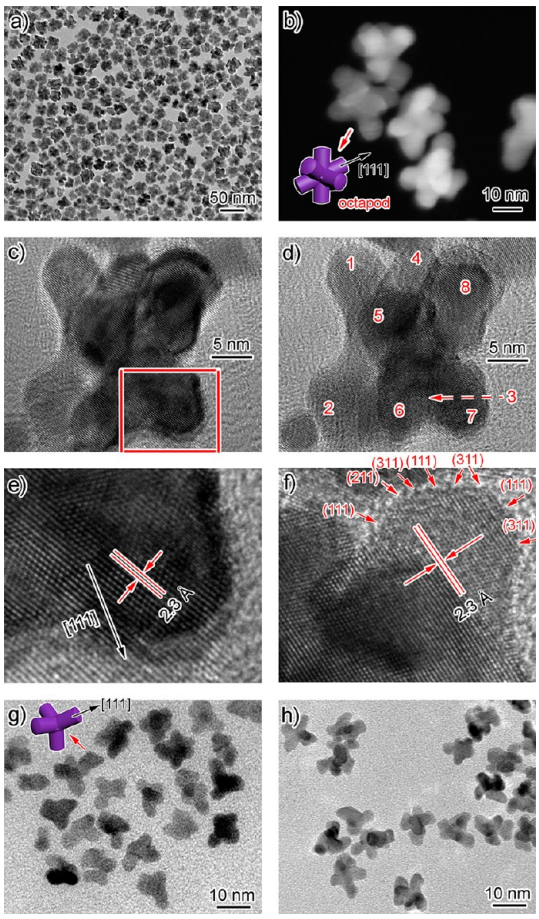

Figure 4. TEM, STEM and HRTEM images of the octopod sample prepared in the presence of 675 mM HCl for 24 h: (a) TEM image; (b) STEM image; (c−f) HRTEM images. The inset of panel b shows the schematics of a typical nanoparticle in the image. The numeric labels in the HRTEM image d illustrate the numbers of branches. (d) Image of the nanoparticle in panel c recorded by tilting 15°. (f) Highlights of the stepped surface atoms on a pod. (e) Magnified image of the region marked by the red box in panel c. (g, h) TEM image and structure schematics of the intermediate product formed at 30 min and 2 h, respectively.

identify the stage of cuboctahedral seeds; however, we captured the intermediates of tetrapods from the reaction at 30 min and 2 h, respectively (see Figures 4g and 4h). It implies that octopods evolve from the precursors of tetrapods *via* atomic addition on the four insufficiently grown {111} faces (namely "Growth Pattern 4" in our work). In other words, the difference in the growth modes for tetrapods and octopods (Pattern 2 *versus* Pattern 4) lies on whether atomic addition occurs on only four {111} faces or all the eight {111} faces. In principle, this atomic addition may be affected by the surface activation of seeds or/and the supply kinetics of freshly formed atoms in solution. The statistics of branched morphologies in each sample is shown in the histograms in Figure 5. The criteria to determine the shape of branched structures in the histograms is based on the numbers of main branches, counting from 80 to 180 particles, regardless of the particle sizes or sub-branched growth.

From the experimental observations above, we can conclude that the final morphologies of products may be determined by three factors in turn: (i) the crystallinity of seeds and nanocrystals; (ii) the number of {111} or {100} faces provided for growth sites; (iii) the supply kinetics of freshly formed Pt atoms. Note that the factors (ii) and (iii) determine the process of atomic addition on seeds in the formation of Pt nanocrystals. Our experiments clearly show that HCl plays an important role in affecting these three factors, as it has been verified that the concentration of HCl is a major parameter for determining the number of branches in multipod structures. As a necessary supplement to Figures 1−4, the more data points in Supporting Information, Figure S1 show the trend for morphological dependence on HCl more clearly. Taken together with the images in Figures 1−4, they reveal the morphological variation from tripods to tetrapods, hexapods, and then octopods by gradually increasing the amounts of HCl. Previously we have demonstrated that oxygen and chloride (O_2/Cl^- pair) can induce oxidative etching.[39−41] In particular, the potential of oxygen reduction is increased from 0.401 to 1.229 V depending on the concentration of acid, which makes the etching effect more significant.[42] Thus the presence

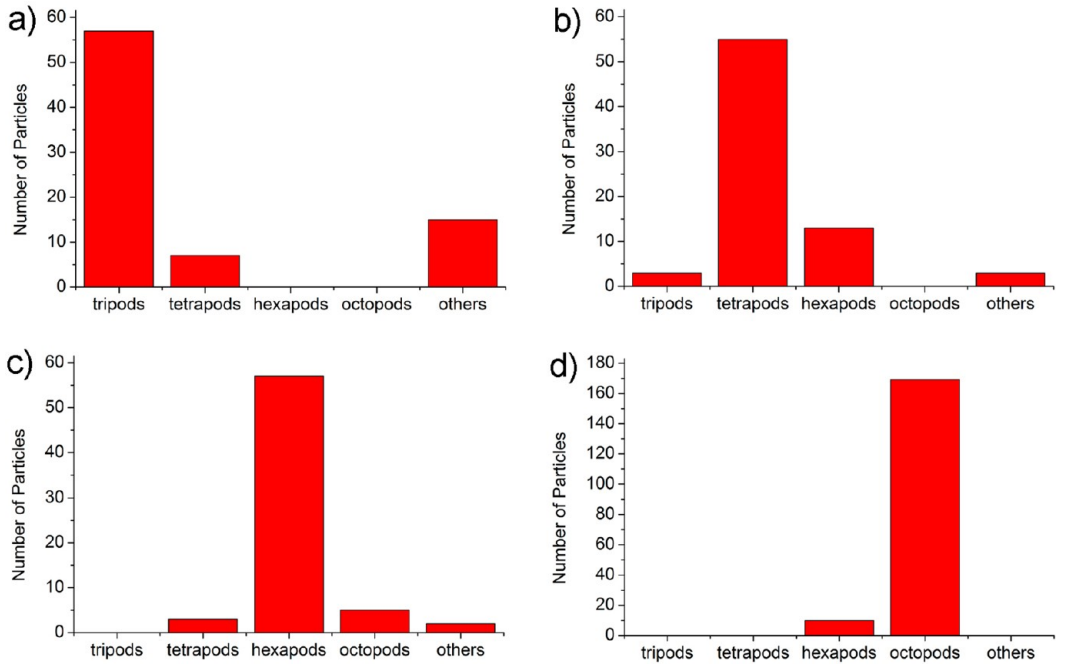

Figure 5. Histogram for the nanoparticles of different shapes in the samples: (a) sample in Figure 1a; (b) sample in Figure 2a; (c) sample in Figure 3a; (d) sample in Figure 4a.

of acid can facilitate the oxidative etching process. It has been verified in our previous studies that defect zones in twinned seeds are much higher in energy relative to single-crystal counterparts, so their atoms can be attacked by the etchant and dissolved into the solution due to oxidative etching.[39] Thus the addition of HCl can tune the crystallinity of seeds and nanocrystals from single twin to single crystal in our case (*i.e.*, alter from Pattern 1 to Patterns 2−4). On the other hand, it appears that HCl can impact the atomic addition onto single-crystal seeds—the number of branches is tuned from 4 to 6 and then to 8 by increasing the concentration of HCl. As mentioned above, this atomic addition should be related to two factors: surface facets provided for atomic addition, and kinetics of atomic supply. For the second factor, there is little doubt that oxidative etching by HCl can control the kinetics of atomic generation. It has been previously demonstrated that the generation of freshly formed atoms can be slowed by etching, affecting the rate of atomic addition.[40,41] Thus basically the kinetics of atomic supply and atomic addition can be effectively tuned, when the concentration of HCl is altered. The importance of oxidative etching in eliminating twinned structures and affecting atomic addition has been demonstrated by control experiments by eliminating acid and/or bubbling argon gas (see Figure 6). Ideally oxidative etching can be greatly suppressed in the absence of oxygen and/or acid. In the present case, the addition of argon gas could not completely eliminate oxygen from the system, since oxygen has a strong binding to the platinum surface. Thus essentially the use of argon gas only reduces the amount of

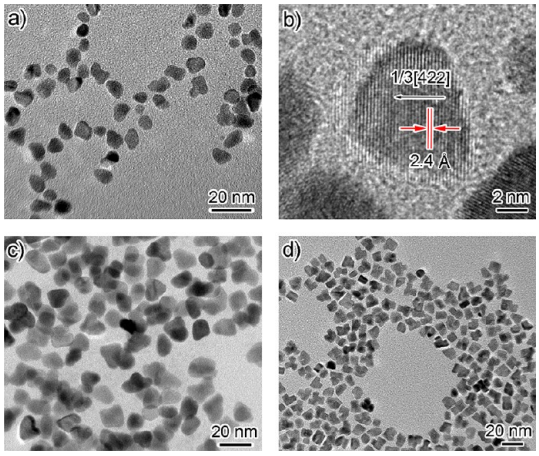

Figure 6. TEM images of the samples prepared under the same condition as that in Figure 4a (*i.e.*, prepared in the presence of 675 mM HCl in air for 24 h), except for the difference as follows: (a,b) the use of NaCl (675 mM) instead of HCl and the Ar environment instead of air; (c) the Ar environment instead of air; (d) the use of NaCl (675 mM) instead of HCl.

oxygen in the reaction system. As a result, the effect of oxidative etching is relatively weakened by the elimination of acid and/or the reduction of oxygen amount from the reaction. Under these conditions, the obtained nanocrystals are mostly planar and single-twinned. Although a small portion of nanoparticles is single-crystal, their branched growth is very limited. It indicates that the oxidative etching is the major contributor to eliminating the twinned structures and controlling the branched growth. However, the major question for the mechanism in our work comes from the first factor—surface facets provided for atomic

addition. To elucidate how HCl affects this factor, it is necessary to investigate the role of the capping effect from bromide and other species.

It has been demonstrated that bromide can selectively adsorb onto the Pt and Pd {100} surface and thus alter surface free energies.[41] In the present case, it is assumed that bromide plays the same role in capping the {100} surface facets on Pt cuboctahedral seeds. As a result, atomic addition prefers to selectively occur on the {111} corners of cuboctahedral seeds rather than all over the surface (particularly when the concentration of additional HCl is kept low). Taken together, it is believed that two key components make major contributions to the formation of various branched nanocrystals: oxidative etching induced by HCl, and protection of {100} facets by bromide. In the absence of HCl, the role of oxidative etching is negligible, so single-twinned seeds can be formed in the early stage. As the side {100} faces of planar seeds are covered by bromide, further atomic addition will occur on the tips of side {111} faces, leading to the production of Pt tripods (*i.e.*, Growth Pattern 1). As HCl is introduced to the reaction, oxidative etching will eliminate the formation of twinned structures. Thus small single-crystal nanoparticles enclosed by a mix of {111} and {100} facets are initially formed in solution, as the spherical shapes (or Wulff polyhedrons) are most favored by thermodynamics in order to minimize the total surface energies.[22−24] According to the literature, the morphology of a nanocrystal depends on the diffusion rate (V_1) of precursor from solution to the surface and the growth rate (V_2) at which atoms are generated and added to the surface of a growing seed in a kinetically controlled synthesis.[42] In our case, the V_1 is controlled by the supply rate of Pt atoms from solution. The supply of Pt atoms (essentially the generation of free Pt atoms) is manipulated by oxidative etching. With the increase of HCl concentrations, the oxidative etching is enhanced to suppress the supply of Pt atoms. The V_2 highly depends on the surface condition of seeds. At a high concentration of bromide, the {100} surface is well protected (de-energized) and thus further atomic addition preferentially occurs on the {111} corners. As demonstrated above, the reaction rate can be tuned by oxidative etching, depending on the amount of HCl. At a relatively fast reaction rate (*i.e.*, in the case of low HCl concentration), most Pt stock is consumed in the early stage so the rest of the freshly formed Pt atoms are only sufficient for the atomic addition on half of the {111} surface. As a result, Pt tetrapods can be formed *via* Growth Pattern 2. As more HCl is added, the generation of Pt atoms is suppressed prior to the starting point of branched growth. In this case, more Pt stock can be saved for the successive branched growth in a relatively long period of time. On the other hand, when the oxidative etching is enhanced, it can facilitate the surface reactivation of {100} facets by removing bromide from the surface. This feature has been observed in our previous work.[41] As a result, both {111} and {100} surface facets are exposed for atomic addition. In terms of surface free energies, low-index facets have the order of $\gamma_{(111)} < \gamma_{(100)} < \gamma_{(110)}$. Thus the atomic addition preferentially occurs on the {100} facets, leading to the formation of hexapods (*i.e.*, Growth Pattern 3). As the concentration of HCl reaches a certain level (*e.g.*, 675 mM), HCl not only increases the strength of oxidative etching, but also introduces a significant amount of chloride into the solution. Chloride has a similar capping effect on {100} facets of Pt to bromide.[43] As reported in literature, the strength of chemisorption or surface coordination to Pt surface increases in the order of chloride < bromide < iodide.[43] This weak capping effect of chloride has been proven by control experiments (see Supporting Information, Figure S2). At a low concentration of chloride, its adsorption is not strong enough for surface capping; however, the huge increase in its concentration would make its {100} capping effect more significant. In this case, {100} facets should have been notably deactivated from atomic addition, according to the growth pattern determined by the HRTEM observations above. We assume that chloride has a significant capping effect on {100} faces in this case. As a result, the surface condition of seeds is quite identical to that in Growth Pattern 2. However, the kinetics of atomic generation in the Growth Pattern 4 is much slower in comparison with Pattern 2. At a very high concentration of HCl, the supply of Pt atoms is so slow that cuboctahedral seeds can gradually grow into tetrapods and then octopods (*i.e.*, Growth Pattern 4) when freshly formed Pt atoms are added to the {111} corners. Certainly, the final overall sizes of nanocrystals should be increased with the enhancement of oxidative etching, which has been verified by TEM observations in Figures 1−4.

The tunable structures of Pt branched nanocrystals offer a platform to investigate the effect of branches on their catalytic performance. We have employed the electrocatalytic oxidation of formic acid for comparison studies on branched structures. The blank CVs of all the samples clearly show the presence of adsorption states of H to (110) and (100) step sites at 0.12 and 0.26 V, respectively, which is superimposed with a broad current wave from H adsorption at (111) sites (see Figure 7).[6] The clear double-layer region and the well-defined current peaks for H adsorption/desorption indicate that the measurements of electrocatalytic performance of samples in Figure 7 are not affected by contaminants such as PVP, chloride, bromide, and ethylene glycol. The active surface area of all the samples can be acquired by analyzing this set of blank CVs, which is further used to normalize the electrocatalytic CVs in Figure 8b. From the CVs, we also noticed the broader double-layer region (charging and

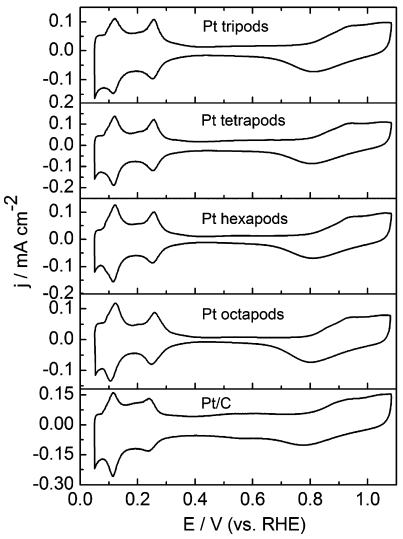

Figure 7. Cyclic voltammograms of electrodes composed of Pt tripods, tetrapods, hexapods, and octopods, respectively, in 0.5 M H_2SO_4 solution at a scan rate of 50 mV/s.

discharging) in the case of Pt/C, which should be mainly contributed by the higher capacitance from carbon support in the catalysts.[44]

Figure 8a shows the mass activities of all the samples toward formic acid oxidation. The maximum current densities of formic acid oxidation are in the order of octopod > hexapod > tetrapod > tripod, indicating that the electrocatalytic performance of branched structures can be improved by increasing the branch number. It should be noticed that the samples have been characterized with XPS prior to transferring them onto electrodes (Supporting Information, Figure S3) and after electrochemical cleaning process (Figure S4), respectively. It verifies that all the samples are free of chloride and bromide after the electrochemical cleaning within the detection limit of XPS technique, although a very small amount of bromide was found prior to the cleaning step. All the results indicate that the measurements of electrocatalytic performance of samples are not affected by contaminants such as PVP, chloride, bromide, and ethylene glycol. In the assessment of electrocatalytic activities, we have to address that the effect from surface area is not the major contributor to tuning their electrocatalytic activities. The active surface area of all the samples that can be estimated from the charges for the oxidation of H adlayer in the potential region from 0.05 to 0.4 V in the blank CVs is summarized in Table 1, from which one can see that the active surface area is increased from 0.39 to 1.32 cm^2 by tuning the number of branches. To exclude the effect from surface area, we have normalized the voltammograms by the active surface area of catalysts. Figure 8b shows the CVs of all the samples toward formic acid oxidation, where the current is normalized by the active surface area of catalysts. The maximum current densities of formic acid oxidation

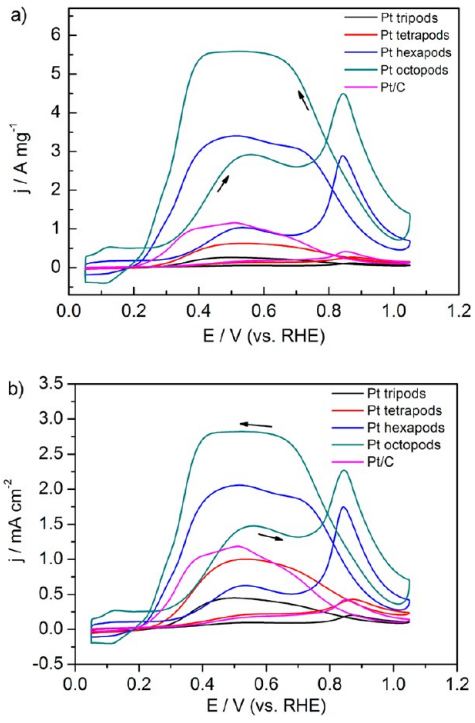

Figure 8. Cyclic voltammograms for formic acid oxidation at electrodes composed of Pt tripods, tetrapods, hexapods, and octopods, respectively: (a) mass-specific activities; (b) surface area-specific activities. Electrolyte, 0.5 M H_2SO_4 + 0.1 M HCOOH solution; scan rate, 50 mV/s.

TABLE 1. The Geometric Area, Active Surface Area and Roughness (Roughness = Active Surface Area/Geometric Area) of the Glassy Carbon Electrodes That Were Modified by Pt Catalysts in Formic Acid Oxidation

Pt nanoparticles	mass loading ($\mu g \cdot cm^{-2}$)	geometric area (cm^2)	active surface area (cm^2)	roughness
Pt tripods	9.455	0.07065	0.39387	5.57495
Pt tetrapods	9.455	0.07065	0.41998	5.94452
Pt hexapods	9.455	0.07065	1.10460	15.63486
Pt octopods	9.455	0.07065	1.32153	18.70530
Pt/C catalysts	9.455	0.07065	0.65147	9.22105

at the tripods, tetrapods, hexapods, and octopods from the positive scans are 0.45, 1.00, 2.07, and 2.81 $mA \cdot cm^{-2}$, respectively. In addition, the onset potential for formic acid oxidation is slightly negatively shifted in the order of octopod > hexapod > tetrapod > tripod, indicating the improvement of electrocatalytic activities at octopods.[5,45] Furthermore, the significant current at potentials below 0.35 V is observed at hexapods and octopods, indicating that such catalysts have high tolerance toward CO poisoning. These results clearly demonstrate that the catalytic activity of Pt nanocrystals can be improved by building complex branched structures, although their particle sizes are increased from 12 to 22 nm meanwhile. The catalytic activities of Pt hexapods and octopods developed in the present work are better than that of commercial Pt/C catalysts

(*versus* 1.19 mA·cm^{-2}) and other complex structures (see Supporting Information, Figure S5).[6,46] The activity enhancement is most likely related to the unique surface structures of branched nanocrystals. From Figure 4f, one can see that there are high densities of stepped surface atoms on the octopods, which is supposed to exhibit higher catalytic activity.[5] Further investigations are underway to fully understand the structure−activity relationship.

CONCLUSION

We have developed a simple synthetic system that allows the numbers and dimensions of branches in Pt nanocrystals to be tailored by tuning the concentration of additional HCl. HCl plays triple functions in tuning branched structures *via* oxidative etching: (i) the crystallinity of seeds and nanocrystals; (ii) the number of {111} or {100} faces provided for growth sites; (iii) the supply kinetics of freshly formed Pt atoms in solution. It enables the acquisition of tunable branched structures with identical chemical environment for catalytic studies, since different growth patterns can be all observed in this system. Among various branched structures, Pt octopods exhibited superior electrocatalytic performance as compared with their counterparts and commercial Pt/C catalysts. It is anticipated that this work will open a door to design complex nanostructures and to achieve specific functions for various applications.

EXPERIMENTAL SECTION

Synthesis. In a typical synthesis, 5 mL of ethylene glycol (EG, Aladdin, 1095698−500 mL) was hosted in a 25-mL, 3-neck flask (equipped with a reflux condenser and a Teflon-coated magnetic stirring bar) and heated in air under magnetic stirring at 116 °C. Meanwhile, 0.0677 g of chloroplatinic acid hydrate (H_2PtCl_6, Aldrich, 254029-1G) and a different amount of hydrochloric acid (HCl) were dissolved in 3 mL of EG; 0.600 g of KBr, and 0.0916 g of poly(vinyl pyrrolidone) (PVP, M.W.= 55 000, Sigma-Aldrich, 856568, 100 g) were dissolved in 3 mL of water at room temperature. The molar ratio of $[PtCl_6]^{2-}$ to Br^- and the repeating unit of PVP was kept as 1:30:15. The aqueous stock solution was then quickly injected into the flask, followed by the addition of EG stock solution. The reaction mixture was heated at 116 °C in air for different periods of time, and sets of samples were taken over the course of each synthesis with a glass pipet. The final products from all the syntheses were collected at t = 24 h. The product was collected by centrifugation and washed with acetone once, ethanol three times, and water four times to remove most of the EG and excess PVP. The as-obtained samples were then characterized by TEM, STEM, and HRTEM.

Morphology Characterization. A drop of the aqueous suspension of particles was placed on a piece of carbon-coated copper grid and dried under ambient conditions. TEM images were taken on a JEOL JEM-2010 LaB6 high-resolution transmission electron microscope operated at 200 kV. STEM and HRTEM images were taken on a JEOL JEM-2100F field-emission high-resolution transmission electron microscope operated at 200 kV.

XPS Characterization. To verify that all the four samples are free of chloride and bromide in the electrochemical measurements, X-ray photoelectron spectra (XPS) were collected on an ESCALab 250 X-ray photoelectron spectrometer, using nonmonochromatized Al−Kα X-ray as the excitation source.

Electrochemical Measurements. The electrochemical measurements were performed at room temperature. The catalysts dispersed onto a glassy carbon electrode (GCE) were used as a working electrode (WE). To prepare the WE, 4 μL of an aqueous suspension of the nanoparticles (167 μg/mL) was transferred to the GCE with a geometric area of 0.07 cm^2. The nanoparticles were prewashed with acetone once, ethanol three times, and water four times. Upon drying under air for 3 h, the electrode was cleaned with RF plasma (Plasma Cleaner pdc-002, Harrick, NY, USA) at a power level of 10.5 W for 1.5 min to remove residue organics, and then covered with 3 μL of Nafion dispersed in water (0.025%). A Ag/AgCl electrode and a platinum foil were used as the reference and counter electrode, respectively. Prior to electrocatalytic measurements, hundreds of potential cycles were conducted in 0.5 M H_2SO_4 solution with saturated CO and then in another 0.5 M H_2SO_4 solution with continuous N_2 gas in the potential region from −0.2 to 1.0 V till the blank CVs stay unchanged, in order to let residue organics and ions release. The blank CVs were collected at a sweep rate of 50 mV/s in freshly prepared 0.5 M H_2SO_4 solution. For the electro-oxidation of formic acid, the CVs were recorded at a sweep rate of 50 mV/s in 0.5 M H_2SO_4 + 0.1 M HCOOH. The current was normalized by the active surface area of catalysts estimated from the charges for the oxidation of H adlayer in the potential region from 0.05 to 0.4 V in the blank CVs. Electrode potential was controlled by a CHI 660D electrochemical station (Shanghai Chenhua, China). Commercial Pt/C catalysts (Pt: 40% wt) were used as a reference to evaluate the electrocatalytic performance of samples. The concentration of platinum nanoparticles was measured with a Thermo Scientific PlasmaQuad 3 inductively coupled plasma mass spectrometry (ICP−MS) after dissolving them with a mixture of HCl and HNO_3 (3:1, volume ratio). With the information of nanoparticle concentrations, all the samples were diluted to the concentration of 167 μg/mL.

Conflict of Interest: The authors declare no competing financial interest.

Acknowledgment. This work was financially supported by the National Natural Science Foundation of China (Nos. 21101145, J1030412), the Recruitment Program of Global Experts, the CAS Hundred Talent Program, a pilot grant from the St. Louis Institute of Nanomedicine, and the Fundamental Research Funds for the Central Universities (No. WK2340000017). M.J.K. was supported by a grant from the World-Class University Program (MEST through NRF (R31-10026)). Part of the work was performed in part at the Nano Research Facility (NRF), a member of the National Nanotechnology Infrastructure Network (NNIN), which is supported by the NSF under Award No. ECS-0335765. NRF is part of the School of Engineering and Applied Science at Washington University in St. Louis.

Supporting Information Available: TEM images of the samples obtained from control experiments; XPS characterization of the samples prior to electrochemical measurements; CV curve for a different branched structure. This material is available free of charge *via* the Internet at http://pubs.acs.org.

REFERENCES AND NOTES

1. Rouxoux, A.; Schulz, J.; Patin, H. Reduced Transition Metal Colloids: A Novel Family of Reusable Catalysts? *Chem. Rev.* **2002**, *102*, 3757–3778.
2. William, K. R.; Burstein, G. T. Low Temperature Fuel Cells: Interactions between Catalysts and Engineering Design. *Catal. Today* **1997**, *38*, 401–410.
3. Tsung, C.-K.; Kuhn, J. N.; Huang, W.; Aliaga, C.; Huang, L.-I.; Somorjai, G. A.; Yang, P. Sub-10 nm Platinum Nanocrystals with Size and Shape Control: Catalytic Study for Ethylene and Pyrrole Hydrogenation. *J. Am. Chem. Soc.* **2009**, *131*, 5816–5822.
4. Huang, X.; Zhao, Z.; Fan, J.; Tan, Y.; Zheng, N. Amine-Assisted Synthesis of Concave Polyhedral Platinum Nanocrystals

Having {411} High-Index Facets. *J. Am. Chem. Soc.* **2011**, *133*, 4718–4721.
5. Tian, N.; Zhou, Z.-Y.; Sun, S.-G.; Ding, Y.; Wang, Z. L. Synthesis of Tetrahexahedral Platinum Nanocrystals with High-Index Facets and High Electro-oxidation Activity. *Science* **2007**, *316*, 732–735.
6. Grozovski, V.; Solla-Gullón, J.; Climent, V.; Herrero, E.; Feliu, J. M. Formic Acid Oxidation on Shape-Controlled Pt Nanoparticles Studied by Pulsed Voltammetry. *J. Phys. Chem. C* **2010**, *114*, 13802–13812.
7. Iwasita, T.; Xia, X. H.; Herrero, E.; Liess, H.-D. Early Stages during the Oxidation of HCOOH on Single-Crystal Pt Electrodes as Characterized by Infrared Spectroscopy. *Langmuir* **1996**, *12*, 4260–4265.
8. Hoshi, N.; Kida, K.; Nakamura, M.; Nakada, M.; Osada, K. Structural Effects of Electrochemical Oxidation of Formic Acid on Single Crystal Electrodes of Palladium. *J. Phys. Chem. B* **2006**, *110*, 12480–12484.
9. Arenz, M.; Stamenkovic, V.; Schmidt, T. J.; Wandelt, K.; Ross, P. N.; Markovic, N. M. The Electro-Oxidation of Formic Acid on Pt–Pd Single Crystal Bimetallic Surfaces. *Phys. Chem. Chem. Phys.* **2003**, *5*, 4242–4251.
10. Rodriguez, P.; Herrero, E.; Solla-Gullón, J.; Vidal-Iglesias, F. J.; Aldaz, A.; Feliu, J. M. Specific Surface Reactions for Identification of Platinum Surface Domains: Surface Characterization and Electrocatalytic Tests. *Electrochim. Acta* **2005**, *50*, 4308–4317.
11. Vidal-Iglesias, F. J.; Solla-Gullón, J.; Rodriguez, P.; Herrero, E.; Montiel, V.; Feliu, J. M.; Aldaz, A. Shape-Dependent Electrocatalysis: Ammonia Oxidation on Platinum Nanoparticles with Preferential (100) Surfaces. *Electrochem. Commun.* **2004**, *6*, 1080–1084.
12. Olofsson, G.; Wallenberg, L. R.; Andersson, A. Selective Catalytic Oxidation of Ammonia to Nitrogen at Low Temperature on $Pt/CuO/Al_2O_3$. *J. Catal.* **2005**, *230*, 1–13.
13. Van der Vliet, D.; Wang, C.; Debe, M.; Atanasoski, R.; Markovic, N. M.; Stamenkovica, V. R. Platinum-Alloy Nanostructured Thin film Catalysts for the Oxygen Reduction Reaction. *Electrochim. Acta* **2011**, *56*, 8695–8699.
14. Bonakdarpour, A.; Dahn, T. R.; Atanasoski, R. T.; Debe, M. K.; Dahn, J. R. H_2O_2 Release during Oxygen Reduction Reaction on Pt Nanoparticles. *Electrochem. Solid State Lett.* **2008**, *11*, B208–B211.
15. Mazumder, V.; Chi, M. F.; More, K. L.; Sun, S. H. Core/Shell Pd/FePt Nanoparticles as an Active and Durable Catalyst for the Oxygen Reduction Reaction. *J. Am. Chem. Soc.* **2010**, *132*, 7848–7849.
16. Gutierrez de Dios, F. J.; Gomez, R.; Feliu, J. M. Preparation and Elecrocatalytic Activity of Rh Adlayers on Pt(100) Electrodes: Reduction of Nitrous Oxide. *Electrochem. Commun.* **2001**, *3*, 659–664.
17. Duca, M.; Cucarella, M. O.; Rodriguez, P.; Koper, Marc T. M. Direct Reduction of Nitrite to N_2 on a Pt(100) Electrode in Alkaline Media. *J. Am. Chem. Soc.* **2010**, *132*, 18042–18044.
18. Duca, M.; Figueiredo, M. C.; Climent, V.; Rodriguez, P.; Feliu, J. M.; Koper, Marc T. M. Selective Catalytic Reduction at Quasi-perfect Pt(100) Domains: A Universal Low-Temperature Pathway from Nitrite to N_2. *J. Am. Chem. Soc.* **2011**, *133*, 10928–10939.
19. Davis, S. M.; Zaera, F.; Somorjai, G. A. Surface Structure and Temperature Dependence of *N*-Hexane Skeletal Rearrangement Reactions Catalyzed over Platinum Single Crystal Surfaces: Marked Structure Sensitivity of Aromatization. *J. Catal.* **1984**, *85*, 206–223.
20. Lee, H.; Habas, S. E.; Kweskin, S.; Butcher, D.; Somorjai, G. A.; Yang, P. Morphological Control of Catalytically Active Platinum Nanocrystals. *Angew. Chem., Int. Ed.* **2006**, *45*, 7824–7828.
21. Bratlie, K. M.; Lee, H.; Komvopoulos, K.; Yang, P.; Somorjai, G. A. Platinum Nanoparticle Shape Effects on Benzene Hydrogenation Selectivity. *Nano Lett.* **2007**, *7*, 3097–3101.
22. Xia, Y.; Xiong, Y.; Lim, B.; Skrabalak, S. E. Shape-Controlled Synthesis of Metal Nanocrystals: Simple Chemistry Meets Complex Physics? *Angew. Chem., Int. Ed.* **2009**, *48*, 60–103.
23. Tao, A.; Habas, S.; Yang, P. Shape Control of Colloidal Metal Nanocrystals. *Small* **2008**, *4*, 310–325.
24. Chen, J.; Lim, B. K.; Lee, E. P.; Xia, Y. Shape-Controlled Synthesis of Platinum Nanocrystals for Catalytic and Electrocatalytic Applications. *Nano Today* **2009**, *4*, 81–95.
25. Lim, B.; Xia, Y. Metal Nanocrystals with Highly Branched Morphologies. *Angew. Chem., Int. Ed.* **2011**, *50*, 76–85.
26. Maksimuk, S.; Teng, X.; Yang, H. Roles of Twin Defects in the Formation of Platinum Multipod Nanocrystals. *J. Phys. Chem. C* **2007**, *111*, 14312–14319.
27. Manna, L.; Milliron, D. J.; Meisel, A.; Scher, E. C.; Alivisatos, A. P. Controlled Growth of Tetrapod-Branched Inorganic Nanocrystals. *Nat. Mater.* **2003**, *2*, 382–385.
28. Chen, M.; Xie, Y.; Lu, J.; Xiong, Y.; Zhang, S.; Qian, Y.; Liu, X. Synthesis of Rod-, Twinrod-, and Tetrapod-Shaped CdS Nanocrystals Using a Highly Oriented Solvothermal Recrystallization Technique. *J. Mater. Chem.* **2002**, *12*, 748–753.
29. Milliron, D. J.; Hughes, S. M.; Cui, Y.; Manna, L.; Li, J.; Wang, L.-W.; Alivisatos, A. P. Colloidal Nanocrystal Heterostructures with Linear and Branched Topology. *Nature* **2004**, *430*, 190–195.
30. Mahmoud, M. A.; Tabor, C. E.; El-Sayed, M. A.; Ding, Y.; Wang, Z.-L. A New Catalytically Active Colloidal Platinum Nanocatalyst: The Multiarmed Nanostar Single Crystal. *J. Am. Chem. Soc.* **2008**, *130*, 4590–4591.
31. Lim, B.; Jiang, M.; Camargo, P. H. C.; Cho, E. C.; Tao, J.; Lu, X.; Zhu, Y.; Xia, Y. Pd–Pt Bimetallic Nanodendrites with High Activity for Oxygen Reduction. *Science* **2009**, *324*, 1302–1305.
32. Teng, X.; Yang, H. Synthesis of Platinum Multipods: An Induced Anisotropic Growth. *Nano Lett.* **2005**, *5*, 885–891.
33. Lim, S. I.; Ojea-Jiménez, I.; Varon, M.; Casals, E.; Arbiol, J.; Puntes, V. Synthesis of Platinum Cubes, Polypods, Cuboctahedrons, and Raspberries Assisted by Cobalt Nanocrystals. *Nano Lett.* **2010**, *10*, 964–973.
34. Chen, J.; Herricks, T.; Xia, Y. Poly Synthesis of Platinum Nanostructures: Control of Morphology through the Manipulation of Reduction Kinetics. *Angew. Chem., Int. Ed.* **2005**, *44*, 2589–2592.
35. Kirkland, A. I.; Jefferson, D. A.; Duff, D. G.; Edwards, P. P.; Gameson, I.; Johnson, B. F. G.; Smith, D. J. Structural Studies of Trigonal Lamellar Particles of Gold and Silver. *Proc. R. Soc. London, A* **1993**, *440*, 589–609.
36. Xiong, Y.; McLellan, J. M.; Chen, J.; Yin, Y.; Li, Z.-Y.; Xia, Y. Kinetically Controlled Synthesis of Triangular and Hexagonal Nanoplates of Palladium and Their SPR/SERS Properties. *J. Am. Chem. Soc.* **2005**, *127*, 17118–17127.
37. Xiong, Y.; Washio, I.; Chen, J.; Cai, H.; Li, Z.-Y.; Xia, Y. Poly(vinyl pyrrolidone): A Dual Functional Reductant and Stabilizer for the Facile Synthesis of Noble Metal Nanoplates in Aqueous Solutions. *Langmuir* **2006**, *22*, 8563–8570.
38. Xiong, Y.; Siekkinen, A. R.; Wang, J.; Yin, Y.; Kim, M. J.; Xia, Y. Synthesis of Silver Nanoplates at High Yields by Slowing Down the Polyol Reduction of Silver Nitrate with Polyacrylamide. *J. Mater. Chem.* **2007**, *17*, 2600–2602.
39. Xiong, Y.; Chen, J.; Wiley, B.; Xia, Y.; Aloni, S.; Yin, Y. Understanding the Role of Oxidative Etching in the Polyol Synthesis of Pd Nanoparticles with Uniform Shape and Size. *J. Am. Chem. Soc.* **2005**, *127*, 7332–7333.
40. Xiong, Y.; Chen, J.; Wiley, B.; Xia, Y.; Yin, Y.; Li, Z.-Y. Size-Dependence of Surface Plasmon Resonance and Oxidation for Pd Nanocubes Synthesized *via* a Seed Etching Process. *Nano Lett.* **2005**, *5*, 1237–1242.
41. Xiong, Y.; Cai, H.; Wiley, B. J.; Wang, J.; Kim, M.; Xia, Y. Synthesis and Mechanistic Study of Palladium Nanobars and Nanorods. *J. Am. Chem. Soc.* **2007**, *129*, 3665–3675.
42. Chernov, A. A. Theory of the Stability of Face Forms of Crystals. *Sov. Phys. Cryst.* **1972**, *16*, 734–753.
43. Carrasquillo, A.; Jeng, J. J.; Barriga, R. J.; Temesghen, W. F.; Soriaga, M. P. Electrode-Surface Coordination Chemistry: Ligand Substitution and Competitive Coordination of Halides at Well-Defined Pd(100) and Pd(111) Single Crystals. *Inorg. Chim. Acta* **1997**, *255*, 249–254.
44. Bard, A. J.; Faulkner, L. R. *Electrochemical Methods: Fundamentals and Applications*, 2nd ed.; John Wiley & Sons: New York, 2001; p 543–579.

45. Rice, C.; Ha, S.; Masel, R. I.; Waszczuk, P.; Wieckowski, A.; Barnard, T. Direct Formic Acid Fuel Cells. *J. Power Source* **2002**, *111*, 83–89.
46. Kang, Y.; Qi, L.; Li, M.; Diaz, R. E.; Su, D.; Adzic, R. R.; Stach, E.; Li, J.; Murray, C. B. Highly Active Pt_3Pb and Core-Shell Pt_3Pb–Pt Electrocatalysts for Formic Acid Oxidation. *ACS Nano* **2012**, *6*, 2818–2825.